POLITECNICO DI TORINO
Repository ISTITUZIONALE

Anomalous Nernst Effect in Co_xPd_1-x alloy films

Original
Anomalous Nernst Effect in Co_xPd_1-x alloy films / Cabassi, R., Tesi, G., Bernasconi, R., Casoli, F.. - In: JPHYS MATERIALS. - ISSN 2515-7639. - 9:3(2026), pp. 1-10. [10.1088/2515-7639/ae7b8a]

Availability:
This version is available at: 11583/3015315 since: 2026-09-09T09:48:12Z

Publisher:
IOP Publishing

Published
DOI:10.1088/2515-7639/ae7b8a

Terms of use:

This article is made available under terms and conditions as specified in the corresponding bibliographic description in the repository

Publisher copyright

(Article begins on next page)

27 November 2026

JPhys Materials

PURPOSE-LED PUBLISHING™

PAPER • OPEN ACCESS

Anomalous Nernst Effect in Co_xPd_{1-x} alloy films

To cite this article: R Cabassi *et al* 2026 *J. Phys. Mater.* **9** 035008

View the article online for updates and enhancements.

You may also like

- Recent advances in conducting polymer chemiresistive sensors for ammonia gas detection: materials, characterization, and applications
Annelot Nijkoops, Manuela Ciocca, Martina Aurora Costa Angeli et al.
- Epitaxial growth and magnetic phase transitions in non-centrosymmetric $EuPdSi_3$ thin films
Sebastian Kölsch, Alfons G Schuck, Olena Fedchenko et al.
- Coordination flexibility as key factor for variability of local structure in amorphous Zn–Sn–O and Cu–Sn–O thin films
Corvin Krohn, Arne Jörns, Sofie Vogt et al.

This content was downloaded from IP address 78.208.79.125 on 09/09/2026 at 10:42

Journal of Physics: Materials

Check for updates

OPEN ACCESS

RECEIVED
5 March 2026

REVISED
21 May 2026

ACCEPTED FOR PUBLICATION
10 June 2026

PUBLISHED
16 July 2026

Original content from this work may be used under the terms of the Creative Commons Attribution 4.0 licence.

Any further distribution of this work must maintain attribution to the author(s) and the title of the work, journal citation and DOI.

PAPER

Anomalous Nernst Effect in Co_xPd_{1-x} alloy films

R Cabassi[1,*], G Tesi[1,2,3], R Bernasconi[4] and F Casoli[1]

[1] Istituto dei Materiali per Elettronica e Magnetismo-CNR, Parco Area delle Scienze 37/A, 43124 Parma, Italy
[2] Istituto Nazionale di Ricerca Metrologica, Strada delle Cacce 91, 10135 Turin, Italy
[3] Politecnico di Torino, DISAT,Corso Duca degli Abruzzi, 24, 10129 Torino, Italy
[4] Politecnico di Milano Dipartimento di Chimica, Materiali e Ingegneria Chimica 'Giulio Natta', Via Bassini 6, 20133 Milano, Italy
* Author to whom any correspondence should be addressed.

E-mail: riccardo.cabassi@cnr.it

Keywords: energy harvesting, transverse thermoelectric effect, anomalous Nernst effect, magnetic anisotropy, spin–orbit coupling

Supplementary material for this article is available online

Abstract

The anomalous Nernst effect (ANE) in Co_xPd_{1-x} alloy thin films has been investigated for the first time over a range of cobalt concentrations ($x = 0.19 - 0.55$) in samples prepared by electrodeposition. The films were characterized from both the magnetic and thermoelectric point of view, by means of alternating gradient force magnetometry and studying the Nernst and Seebeck effects, in order to assess their suitability for transverse thermoelectric energy conversion. In the adopted experimental setup, maximization of the ANE signal requires a preferential magnetization direction perpendicular to the film plane. It is known that, for this alloy, at co concentrations $x \lesssim 0.4$ the perpendicular magnetic anisotropy overcomes the shape anisotropy; such behavior was verified in the present work through magnetization curves, and correlated with the variations observed in the Nernst signal. The anomalous Nernst coefficient s_{ANE} was found to increase with co concentration, reaching a maximum value of 0.43 $\mu V\,K^{-1}$ for the highest measured cobalt content. The obtained values are comparable with those reported for analogous alloys such as Co_xPt_{1-x}. We have also measured the transverse thermoelectric voltage at zero applied magnetic field s_0, since this would eventually be the figure of interest in practical energy harvesting applications. We have obtained a maximum value of $s_0 = 0.11\ \mu V\,K^{-1}$ at $x = 0.37$, highlighting the fact that the coefficient s_0 is affected not only by the intrinsic ANE value, but also by extrinsic factors.

1. Introduction

While a widespread availability of low voltage power sources will be a primary need of the Internet of Things, the occurrence of low grade wasted heat in many appliances suggests that such need could be fulfilled by the exploitation of thermoelectric effects. The conceivable thermoelectric devices fall into two categories, depending on whether the physical effect at work is *longitudinal* or *transverse*: in the first case the obtained voltage and the thermal gradient are collinear, while in the second case they are perpendicular to each other. In principle, the making of a longitudinal device would just need a thermal gradient to exploit the Seebeck effect, while a transverse device would rely on the Nernst effect and thus a magnetic field would be necessary too. However, though apparently simpler, the longitudinal configuration suffers from some drawbacks with respect to the transverse [1]. In particular, in a Seebeck device an inverse Peltier heat current is generated which degrades the thermal gradient hence the energy conversion efficiency. On the contrary, in a Nernst device an Ettingshausen heat current is generated which reinforces the thermal gradient and improves efficiency. As a result, the attainable conversion efficiency is expected to be more favorable in a transverse device based on the Nernst effect. Despite these considerations, generating a magnetic field is never an effortless task, thus existing thermopiles realized up to now are based on the Seebeck effect [2]. Nonetheless, in recent years much attention has been raised on the possible exploitation of the anomalous Nernst effect (ANE), which would supply transverse thermoelectric effect without the difficulty of generating a magnetic field.

© 2026 The Author(s). Published by IOP Publishing Ltd

The ANE can be seen as the thermoelectric analogue of the anomalous Hall effect (AHE), where the electric potential is replaced by a thermal gradient ∇T. While in AHE the intrinsic contribution is promoted by the effective magnetic field generated by a not-null Berry curvature integrated over all the Bloch bands [3–5], in ANE the integration mainly involves the bands close to the Fermi surface. In ferromagnets such as *f.i.* FePt alloys, Berry-phase-theory calculations show that the intrinsic contribution to ANE comes from the strong spin–orbit coupling of the heavy metal Pt [6]. On the other hand, extrinsic contributions can come from side-jump and skew scattering on impurities and defects [7–9].

In the search for materials exhibting large ANE due to intrinsic mechanisms, different classes have been investigated, mostly hard magnetic alloys for their typically high spin–orbit coupling, but also semi-hard or soft magnetic alloys, and even non-ferromagnetic topological materials for the possible contribution of the Berry curvature [9–12]. Among the materials with sizeable spin–orbit coupling, to the best of our knowledge CoPd alloy was never investigated before, while it could offer a robust zero-field remanent magnetization and be conveniently prepared as thin film by electro-deposition, which offers an alternative route to higher cost physical deposition techniques, such as sputtering deposition [13].

Besides the lack of previous results on ANE performance, the Co–Pd system is interesting for different aspects. In Co_xPd_{1-x} films, the competition between perpendicular magnetocrystalline and shape anisotropy yields preferential direction of magnetization either perpendicular or parallel to the film plane depending on the value of x, with perpendicular anisotropy prevailing for $x \lesssim 0.4$ [14]. Tuning the x values yields also polarity inversion of the AHE, i.e. a sign reversal in the measured Hall voltage, with polarity crossing at $x \simeq 0.4$ [15], a phenomenon observed also in bulk samples with polarity crossing at $x \simeq 0.25$ [16]. The magnetic properties have also been shown to depend strictly on the hydrogen content in the atmosphere, a characteristic that suggested to realize hydrogen sensors based on Co_xPd_{1-x} films [15]. Lastly, Co/Pd multilayers have nearly null interface spin loss, making them appealing for spintronics applications [17].

For what concerns ANE, a tentative, simplified evaluation of the effect could be given considering that the spin–orbit coupling would be provided by Pd, while Co would provide the magnetization necessary to obtain a sizeable voltage: the final result will be given by the trade-off between these two aspects, depending on the x value. One could be tempted to speculate a comparison with CoPt, since Pd and Pt belong the same group of elements. The anomalous Nernst coefficient in Co_xPt_{1-x} films can reach $S_{ANE} = 1.18\ \mu V\ K^{-1}$ for $x = 0.3$ [18], however the d orbital configurations of Pt and Pd, hence their spin–orbit coupling parameters, are different. The spin-Hall angle values of Pd reported in literature range from $\theta_H = 0.005$ to 0.011 [13, 17, 19, 20], to be compared with definitely higher values for Pt ranging from $\theta_H = 0.029$ to 0.080 [17, 21, 22]. Such figures depend very much on the material purity and employed techniques, nonetheless it is reasonable to expect a weaker ANE signal in the Pd alloy compared to the Pt alloy. Clearly, a speculation simply based on the spin–orbit argument cannot be accurate, since ANE effect depends on complex details of the electronic band structure of the alloy, and in particular on the Berry curvature [6], but it has been shown experimentally and supported by first-principle calculations that substituting Pd for Pt in FePt degrades the performance from $S_{ANE} = 0.55\ \mu V\ K^{-1}$ to $0.40\ \mu V\ K^{-1}$ [23]. This is not such a drastic deterioration, a result that plays in favor of investigating the ANE properties of CoPd films. In this work we fill this knowledge gap by measuring the ANE in electro-deposited Co_xPd_{1-x} thin films at different x values, complementing the ANE measurements with thermoelectric and magnetic characterizations.

2. Method

Thin films of Co_xPd_{1-x} were electrodeposited on sapphire and silicon substrates, which were initially coated via magnetron sputtering with a first adhesion layer made of Ti and then with a second conductive layer made of Au. Prior to the sputtering process, the samples were thoroughly cleaned using the following procedure: 5 min sonication in dichloromethane, 5 min sonication in acetone, 5 min sonication in deionized water, 5 min sonication in acetone. Ti and Au were deposited using a HEX system magneton sputtering setup manufactured by Korvus Technology Ltd (UK). Ti was deposited in RF mode, using a 20 sccm flow of Ar, at 200 W power and for 60 s. Au was deposited in DC mode, using a 20 sccm flow of Ar, at 80 mA current and for 75 s. Under these conditions, the expected thickness was 5 nm for Ti and 24 nm for Au. The CoPd alloy was then electrodeposited on the Ti/Au coated samples using an electrolyte originally developed by Takata *et al* [24]. All the chemicals were acquired from Sigma Aldrich and used as received. The composition of the bath was slightly modified in order to get different compositions. Specifically, the concentration of three of the chemicals comprised in the original formulation was kept constant: 0.12 M $PdCl_2 \cdot 2\ H_2O$, 0.6 M glycine, 0.5 M NH_4Cl. $CoCl_2 \cdot 6\ H_2O$, on the

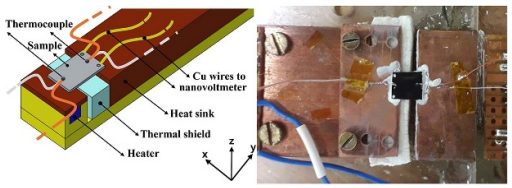

Figure 1. Schematic illustration *(left)* and top view photograph *(right)* of the setup for generation and recording of Nernst voltages. The heater is a 120 Ω resistor above which lays the hot side of the sample. The cold side of the sample lays on a big copper block whose mass is enough to keep it at room temperature. Below and in between the two sides is put a polystyren diaphragm to shield heat transmission from both irradiation and convection. Voltages are brought to a nanovoltmeter through 30 μm wires and the temperatures on hot and cold side are measured by 80 μm diameter thermocouples.

contrary, was varied between 0.024 M and 0.2 M in order to get the following compositions: $x = 0.19$, 0.29, 0.37, 0.39, 0.52, 0.55. The pH was corrected to 6.5 using HCl or NH_4OH and the deposition was carried out at room temperature and in the absence of stirring. A current density equal to 100 mA cm^{-2} was applied for intervals of time between 8 and 12 s. At the end of the deposition process, each sample was thoroughly washed with deionized water and dried with nitrogen. SEM was carried out using an EVO 50 EP setup, manufactured by Zeiss. The instrument was equipped with an energy dispersive spectroscopy unit Inca Energy 200, manufactured by Oxford Instruments. XRD was carried out using a PW1830 diffractometer, manufactured by Philips. The instrument was equipped with $Cu_{K\alpha}$ source and was operated in Bragg-Brentano configuration.

The magnetic properties of the samples were investigated by alternating gradient force magnetometry (AGFM). Hysteresis curves at room temperature were measured by AGFM by applying a maximum field of 2 T, both parallel and perpendicular to the film surface.

The Nernst effect induced by magnetic field loops has been recorded by means of the setup shown in figure 1, which is derived from the concept displayed in the seminal work of Uchida on the Spin Seebeck effect [25]. One side of the film is placed over a heater, while the opposite side is kept cold by a heat sink, thermal contact on both sides is assured by thermal grease. Nernst voltage is measured between the two ends of the cold side by a 2182 Keithley nanovoltmeter, and temperatures have been measured by thermocouples in contact with the film surface, in both cases wirings have been kept as thin as possible (30 μm and 80 μm respectively) in order to avoid heat leakage. The external magnetic field has been generated by an old Newport electromagnet. In the configuration depicted in figure 1, sizeable ANE is expected if remnant magnetization is perpendicular to the film, that is when $x \lesssim 0.4$, according to [14]. It is important to remark that this configuration is appropriate for the case of thermal gradient parallel to the plane of the film while, indeed, many practical applications would be rather focused on thermal gradients perpendicular to the film plane (e.g. energy harvesting from heat dispersed by isothermal surfaces) [1]. The latter case would require in-plane magnetization, which is not treated by our experimental geometry and would be more properly addressed by the heat flux method [26].

Thermal mapping of the film surface has been checked by a Optris OPTPI64ILTMO44T090 infrared camera, aiming at avoiding asymmetries along the direction of voltage measurement, that could induce spurious effects via Seebeck effect. To measure the Seebeck coefficient, one has just to rotate the sample of 90°, move the thermocouples as close as possible to the voltmeters contacts, and repeat the above described procedure.

3. Results

3.1. Morphological characterization

The morphological characterization of some representative CoPd layers was carried out using SEM and the results obtained can be seen in Supporting Information figure S1. The morphology of the samples shows a clear evolution as the content of Co increases. The samples plated at 0.19 and 0.29 as Co molar fraction present evident nodules on the surface, which tend to disappear when the concentration of Co increases. Indeed, they are less evident in the 0.39 sample and absent in the 0.51 sample. This is a consequence of the fact that, according to the Co^{2+}/Pd^{2+} ratio present in the solution, a high amount of Co^{2+} ions favors the deposition rate and improves the uniformity in the case of Co-rich coatings. The cathodic efficiency of the deposition process, and consequently the growth rate of the layer, varies with the composition of the alloy [24, 27]. Considering this aspect, the deposition time was tuned to keep roughly constant the thickness of the coatings, which was determined looking at the cross-sections of the

layers. The thickness presented a relatively small variability, being comprised between 130 and 150 nm. We are confident that thickness uncertainty is not a severe issue for the purposes of the present work, since it has been shown in other ferromagnetic thin film alloys that the thickness dependence of the ANE signal is negligible in this range of values [28].

3.2. XRD characterization

The XRD characterization of some representative CoPd samples evidenced the presence of four sets of reflections. figure S2 shows the result obtained for the coatings with molar fractions of Co comprised between 0.19 and 0.51. Some of the features visible are connected to the presence of the Si substrate and the Ti/Au underlayers. In detail: the peaks identified as A are indicative of the presence of Au, peak B comes from the Si substrate and peak C is probably related to Ti. All these peaks, as expected, can be found exactly in the same position considering the different samples. The peaks identified as *D* are indicative of the presence of fcc CoPd. In conformity with the results previously reported in literature [27, 29], no peaks for the hcp phase of Co were observed, suggesting that Co is fully mixed with Pd to form a fcc lattice. Unlike the other peaks, the CoPd ones (*D*) slightly change position when the amount of Co incorporated in the alloy increases. In the specific case, they move towards the right at higher values of 2θ angle. This behavior is generally well known and widely reported in the case of many alloys obtained by electrodeposition (including CoPd [29]). Indeed, the peaks displace toward higher angles because the material formed is a substitutional solid solution and, when the composition changes, the crystal lattice parameters change as well. The relationship between the crystal lattice parameter a_{CoPd} of fcc CoPd, obtainable from the position of the peaks, and the composition of the alloy is described by the Vegard's law (1)

$$a_{\mathrm{CoPd}} = a_{\mathrm{Co}} x_{\mathrm{Co}} + (1 - x_{\mathrm{Pd}})\, a_{\mathrm{Pd}} \tag{1}$$

where a_{Co} and a_{Pd} are the crystal lattice parameters for fcc Co and Pd, respectively. If the (111) peak (whose position ranges between 40.53° and 41.92°) is considered, the resulting values for a_{CoPd} can be obtained from the Bragg's law and plotted against the molar fraction of Co x_{Co} . The dataset is expanded considering the literature value for a_{Pd} (at x_{Co} equal to 0) and it is represented in figure S3. A clear linear trend can be found from the fitting of the data points, confirming the validity of the Vegard's law and suggesting the formation of a substitutional solid solution, whose crystal lattice varies with the composition. It is also possible to evaluate the dimension of the crystallites exploiting the Scherrer equation (2)

$$D = \frac{K\lambda}{\beta \cos(\theta)} \tag{2}$$

where *D* is the mean size of the ordered crystallites, *K* is a dimensionless shape factor (typically 0.9), λ is the wavelength of the radiation employed, β is the full width at half maximum (FWHM) of the selected peak and θ is its position. The FWHMs of the (111) peaks were corrected subtracting the instrumental line broadening and the resulting values were used to calculate the values of *D*. The obtained results ranged between 8.24 nm and 11.77 nm, which can be considered small crystallites. This is probably a consequence of the relatively high current density employed for the electrodeposition of the CoPd thin layers.

3.3. Magnetization and AHE

Hysteresis magnetic loops, displayed in figure 2 for selected values of *x*, show that in our electrodeposited films the magnetic anisotropy follows the same trend already known for sputtered films, namely the preferential magnetization direction turns from perpendicular to parallel on increasing *x* [14]. For later use in the discussion of results, in figure 3 we also report the values of remanent magnetization at $H = 0$.

The AHE measurements in figure 4 show a sign reversal of the Hall resistivity ρ_H for low *x* values (our available samples allow to estimate a crossover composition between $x = 0.19$ and $x = 0.29$) with increasing ρ_H on increasing *x*, as already observed by other authors [15, 16]. The magnitude of ρ_H is compliant with literature values, and the narrowing of hysteresis widths on increasing *x* is consistent with the weakening of the perpendicular component of ferromagnetism. In particular, comparison of the $x = 0.37$ and the $x = 0.39$ curves highlights the crossing between the two anisotropy regimes.

Considering the above results, we conclude that our films obtained by electrodeposition have reasonably similar behavior with respect to $\mathrm{Co}_x\mathrm{Pd}_{1-x}$ films obtained by sputtering though the latter technique is far less cheap, thus offering an advantage for applications.

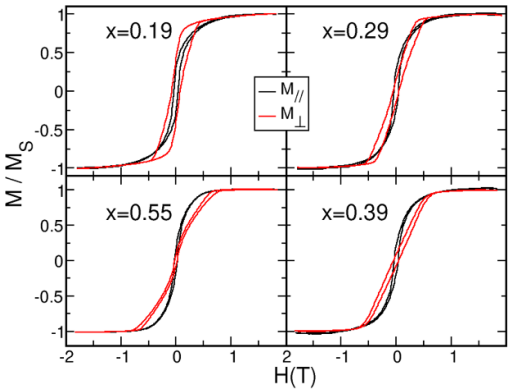

Figure 2. $M-H$ hysteresis loops for selected values of x along the direction parallel (black line) and perpendicular (red line) to the film, showing that the preferential magnetization direction turns from perpendicular to parallel on increasing Co content x.

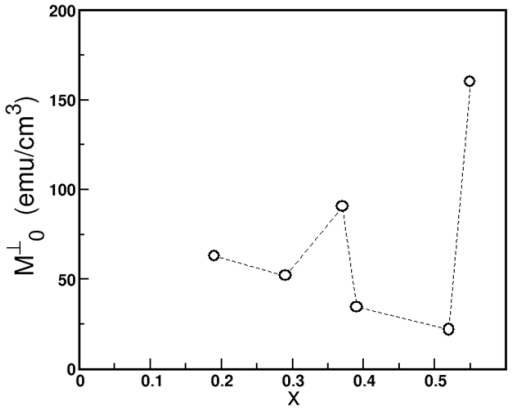

Figure 3. Remanent magnetization M_0 along the direction perpendicular to the film as a function of Co content x.

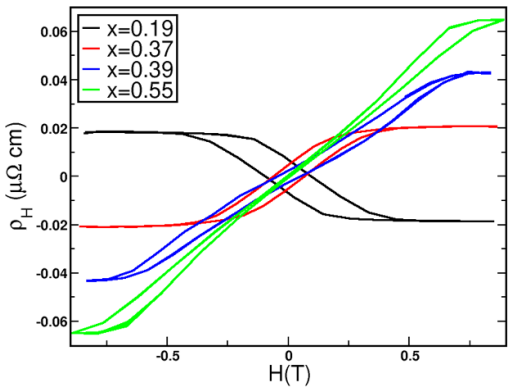

Figure 4. AHE curves for different Co content x values.

3.4. ANE

With the configuration depicted in figure 1, a temperature difference ΔT between the two edges of the film yields a measured transverse voltage given by the sum of two contributions:

$$V = (N\mu_0 H + S_{xz})\,\Delta T. \tag{3}$$

The first term is proportional to the applied magnetic field H through the *normal* Nernst coefficient N, while the second term is the transverse magneto-thermoelectric power object of the present investigation originated by the ANE contribution, which reaches its maximum value at the magnetic saturation $M = M_s$. It is worth noting that while S_{xz} increases on increasing M, it is not necessarily proportional. Moreover, since the magnetization M is an extrinsic property that can change from sample to sample,

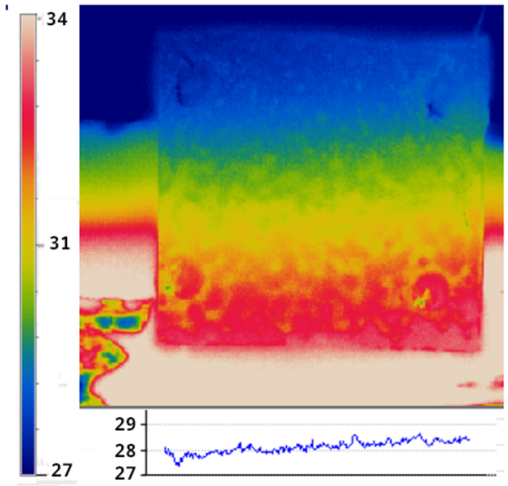

Figure 5. Thermal image of the $x = 0.29$ sample at $\Delta T = 6$ K. The blue line is the temperature profile along the film cold side, showing a temperature difference of $\simeq$0.5 K between the voltmeter contacts.

for material characterization it is usual to refer to the voltage measured at the intrinsic property $M = M_s$. In the materials investigated in this field, the first contribution in equation (3) is usually negligible, anyway, when sizeable, it can be disclosed by the appearing of a linear behavior of the $V(H)$ loop at fields above the magnetic saturation, and easily removed after linear regression of that part of the curve.

Since the measured voltage depends not only on the material properties, but also on the geometry of the system, one defines a normalized anomalous Nernst coefficient expressed in terms of the electric field E and thermal gradient ∇T:

$$S_{\mathrm{ANE}} = \frac{E}{|\nabla T|} = \frac{V}{L_x} \cdot \frac{L_z}{\Delta T} \tag{4}$$

where L_x is the distance between the electric contacts and L_z is the length over which ΔT is applied.

If the two electrodes are not at the very same temperature, the actually measured voltage V can result not only from the transverse Nernst effect, but also from the longitudinal Seebeck effect: for this reason, it is mandatory to obtain a homogeneous thermal profile along the x direction of the film. To check this aspect, before starting measurements we used an infrared camera to take thermal images of the films, one example of which can be seen in figure 5.

The ANE coefficient S_{ANE} is obtained by measuring the Nernst voltage $V(H)$ during magnetic field loops. While in principle the $V(H)$ curves should mimic the magnetic hysteresis loops, as a matter of fact it is normal to observe a bias $\Delta V = (V(0^+) + V(0^-))/2$ along the vertical axis, where the meaning of 0^+ and 0^- is null magnetic field on the rising and descending branch of the hysteresis loop. This is a spurious effect that can be most likely ascribed to Seebeck voltage originating from unavoidable small temperature differences between the two voltmeter contacts. To validate this guess, we have measured the film Seebeck coefficients in order to check if they could give rise to the observed values of ΔV. As an example, the result for the sample $x = 0.29$ is displayed in figure 6: in upper panel, the Seebeck measurements performed as described in section 2 yield a Seebeck coefficient $S_{xx} = 13\mu\mathrm{V\ K}^{-1}$; in lower panel, the ANE measurement recorded at $\Delta T = 6$ K, shows a bias of $\Delta V = 6.1\mu$V. Such value is in excellent agreement with the temperature difference of $\simeq$0.5 K between the voltmeter contacts shown in figure 5, which would yield $\Delta V = S_{xx} \cdot \Delta T = 6.5\ \mu$V. Therefore, in view of ANE investigations the measured $V(H)$ loops will be safely vertically shifted by $-\Delta V$.

The left column in figure 7 shows $V(H)$ loops taken at different ΔT values for selected samples. The anomalous Nernst coefficient S_{ANE} is obtained by reading the voltage at the saturation magnetic field H_{sat}. Taking into account the above discussion about the spurious artifact from Seebeck effect, this has been done on the $V(H)$ loops vertically shifted. In alternative, one could calculate it from the pristine $V(H)$ loops as:

$$S_{\mathrm{ANE}} = \left(V(H_{\mathrm{sat}}) - V(-H_{\mathrm{sat}})\right)/2\Delta T. \tag{5}$$

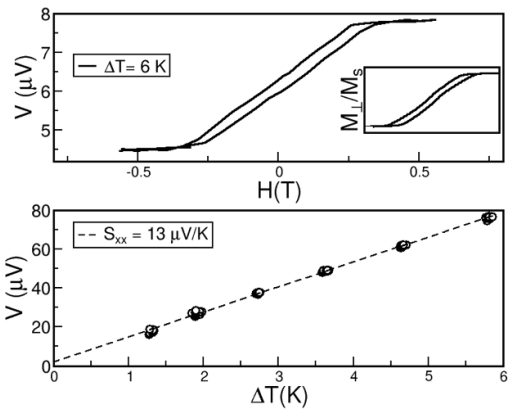

Figure 6. *Upper panel:* ANE measurement of the $x = 0.29$ sample at $\Delta T = 6$ K, corresponding to the IR image of figure 5, the loop suffers of a vertical bias $\Delta V = 6.1\mu$V. *Inset:* the shape of the $M(H)$ loop along the direction perpendicular to the film (from figure 2) mimics the shape of the ANE measurement; *Lower panel:* Seebeck voltage measured at different ΔT values yields a Seebeck coefficient $S = 13\mu$V K^{-1}. For the temperature difference of 0.5 K between the voltmeter contacts recorded in figure 5, this would yield a vertical bias $\Delta V = 6.5\mu$V in the ANE measurement of upper panel.

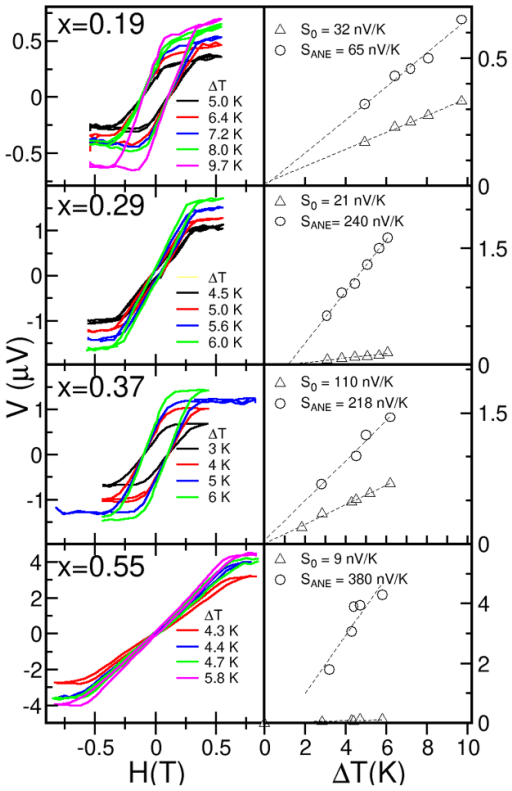

Figure 7. *Lower panel: Left column:* hysteresis loops of the Nernst voltage $V(H)$ taken at different thermal gradients. *Right column:* determination of the transverse thermoelectric thermopower measured at saturation S_{ANE} (circles) and at null magnetic field S_0 (triangles).

In the right column of figure 7, the values of measured V at saturation as function of ΔT are plotted as circular symbols. As expected from equation (4), the data show linear dependence, with slope yielding the value of S_{ANE}.

One comment about the definition of S_{ANE} after normalization by the geometric factor L_z/L_x may be useful. Measuring the ANE voltage at the magnetic saturation is suitable for the study of the intrinsic properties of the material. However, a real device for energy harvesting would work at zero applied magnetic field $H = 0$, rather than at $H = H_{\mathrm{sat}}$. Therefore the performance of a device at working conditions would be better characterized by a new coefficient S_0 obtained by reading the Nernst voltage at $H = 0$:

$$S_0 = \left(V\left(H = 0^{\uparrow}\right) - V\left(H = 0^{\downarrow}\right)\right)/2\Delta T \tag{6}$$

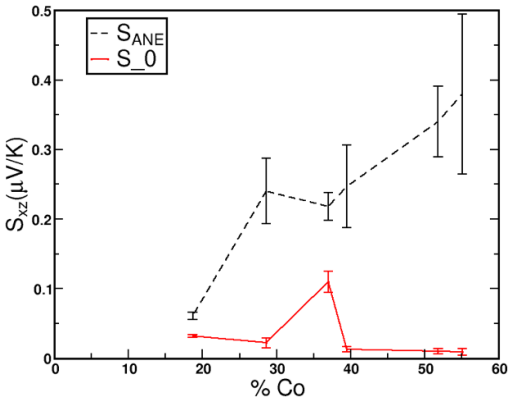

Figure 8. Transverse thermoelectric thermopower measured at saturation S_{ANE} (black dashed line) and measured at null magnetic field S_0 (red continuous line) as a function of the Co content x. Error bars take into account the uncertainty on both the geometric factor L_z/L_x and the linear regressions of figure 7.

where $H = 0^{\uparrow}$ and $H = 0^{\downarrow}$ are the $H = 0$ points on the increasing and decreasing H branch of the $V(H)$ loop respectively. The values of $(V(H = 0^{\uparrow}) - V(H = 0^{\downarrow}))/2$ are plotted as triangular symbols in the right column of figure 7 and, similar to the case of S_{ANE}, show linear dependence with respect to ΔT, with slope yielding S_0. Of course, one always finds $S_0 < S_{ANE}$.

The summary of the S_0 and S_{ANE} values is reported in figure 8. It can be noted that, in the explored range of x, S_{ANE} shows an overall increasing trend on increasing x while, on the contrary, S_0 has a maximum at $x = 0.37$. This is not surprising, since this corresponds to the maximum predominance of perpendicular magnetic anisotropy with respect to shape anisotropy [14], making this the optimal composition for practical applications with in-plane thermal gradient.

4. Discussion and conclusions

We have measured the ANE in Co_xPd_{1-x} thin films obtained by electrodeposition. The quality of the films has been checked by carrying out preliminary structural and magnetic characterizations and comparing the results with some already known properties of this alloy. A specific compositional range, i.e. x from 0.19 to 0.55, has been explored in view of energy harvesting applications with the heat source positioned at one of the lateral sides of the device. In this case, the applied thermal gradient is along the plane of the film and films with easy magnetization direction perpendicular to the plane are most suitable. The greatest transverse thermopower coefficient S_{ANE} has been found for the highest measured Co concentration, namely $S_{ANE} = 0.43\ \mu V\ K^{-1}$. This is lower but comparable with values reported for the Co_xPt_{1-x} alloy, which highlights CoPd alloy as a suitable material for transverse thermoelectric applications. To evaluate this material for the performance for a real device , the thermopower S_0 measured at $H = 0$ would be a more meaningful parameter. For the latter quantity, figure 8 shows values below 0.1 $\mu V\ K^{-1}$, except for the sample with composition $x = 0.37$, which gave the maximum value, i.e. $S_0 = 0.11\ \mu V\ K^{-1}$. The maximum in S_0 is obtained in correspondence with a peak in perpendicular magnetic remanence (figure 3), evidencing that the remanent magnetization contributes to the transverse thermoelectric response at zero field. However, remanent magnetization cannot be identified as the unique origin of the thermopower measured at zero magnetic field, as also indicated by the absence of a complete coherence among the trends of S_0 and M_0 in the whole x range. If we consider the magnetic behavior of the samples with varying x, we can conclude that perpendicular anisotropy decreases with increasing Co-content and perpendicular magnetic remanence is mainly governed by the competition between magnetocrystalline and shape anisotropy (figures 2 and 3). On the other hand, the perpendicular M_0 values do not show a monotonic decrease with increasing x, since also the films with in-plane easy axis show a non-negligible perpendicular remanence and perpendicular remanence values reflects the M_S values, which are in turns affected by Co-content and microstructure. In conclusion, to interpret the S_0 trend as a function of x, we can conclude that different mechanisms are present. As underlined in the introduction, several factors are known to be at play in ANE, both of intrinsic origin, such as spin–orbit effect and Berry-curvature-related mechanisms, and of extrinsic nature, i.e. side-jump and skew scattering from impurities and defects, which are significantly affected by the microstructure of the samples.

As a final remark, the carried-out analysis shows that transverse thermal asymmetries of even a few tenths of degree may yield a voltage bias of magnitude comparable with ANE: this bias can either enhance or weaken the measured voltage, depending on the orientation of the transverse thermal gradient with respect to the film magnetization. The above considerations should be taken into account while choosing the appropriate configuration for practical devices.

Acknowledgments

This project has received funding from the Italian Ministry of University and Research under the Research Projects of Relevant National Interest (PRIN project Xverse T.E.C 'Transverse thermoelectric energy conversion': Grant No. 2022LLWM5F, financed by the European Union-Next Generation EU, mission 4, component 1, CUP B53D23004310006).

Data availability statement

All data that support the findings of this study are included within the article (and any supplementary files).

Supplementary data 1 available at https://doi.org/10.1088/2515-7639/ae7b8a/data1.

Author contributions

R Cabassi 0000-0003-0506-2051
Conceptualization (lead), Data curation (equal), Funding acquisition (equal), Investigation (equal), Methodology (equal), Software (equal), Supervision (equal), Visualization (equal), Writing – original draft (lead), Writing – review & editing (equal)

G Tesi 0009-0006-9486-9939
Conceptualization (equal), Data curation (equal), Investigation (equal), Methodology (equal), Writing – review & editing (equal)

R Bernasconi 0000-0003-2193-8017
Investigation (equal), Methodology (equal), Writing – review & editing (equal)

F Casoli 0000-0002-4323-0362
Data curation (equal), Investigation (equal), Methodology (equal), Writing – review & editing (equal)

References

[1] Mizuguchi M and Nakatsuji S 2019 Energy-harvesting materials based on the anomalous Nernst effect *Sci. Technol. Adv. Mater.* **20** 262–75
[2] Graf A, Arndt M, Sauer M and Gerlach G 2007 Review of micromachined thermopiles for infrared detection *Meas. Sci. Technol.* **18** R59
[3] Acharya G B, Barik S K, Mishra S R, Karki B, Muduli P K, Srinivasan B and Ghimire M P 2025 Berry curvature-driven anomalous Hall effect in polycrystalline ferromagnet Fe5Sn3 *Chem. Mater.* **37** 7419–30
[4] Manna K, Sun Y, Muechler L, Kübler J and Felser C 2018 Heusler Weyl and Berry *Nat. Rev. Mater.* **3** 244–56
[5] Weischenberg J, Freimuth F, Blugel S and Mokrousov Y 2013 Scattering-independent anomalous Nernst effect in ferromagnets *Phys. Rev. B* **87** 060406(R)
[6] Shi Z, Xu S J, Ma L, Zhou S M and Guo G Y 2020 Anomalous Nernst effect in epitaxial L10 FePd1-xPtx alloy films: Berry curvature and thermal spin current *Phys. Rev. Appl.* **13** 054044
[7] Xiao D, Chang M-C and Niu Q 2010 Berry phase effects on electronic properties *Rev. Mod. Phys.* **82** 1959–2007
[8] Zhang H, Xu C Q and Ke X 2021 Topological Nernst effect, anomalous Nernst effect and anomalous thermal Hall effect in the Dirac semimetal *Phys. Rev. B* **103** L201101
[9] Ding L *et al* 2019 Intrinsic anomalous Nernst effect amplified by disorder in a half-metallic semimetal *Phys. Rev. X* **9** 041061
[10] Uchida K, Zhou W and Sakuraba Y 2021 Transverse thermoelectric generation using magnetic materials *Appl. Phys. Lett.* **118** 140504
[11] Liu S, Chen M, Fu C and Zhu T 2023 The interplay of magnetism and thermoelectricity *a review Adv. Phys. Res.* **2** 2300015
[12] Watzman S J, Kikkawa T, Skinner B , Uchida K-I 2025 Utilizing magnetization and spin in thermoelectric applications *MRS Bull.* **50** 915–24
[13] Ando K and Saitoh E 2010 Inverse spin-Hall effect in palladium at room temperature *J. Appl. Phys.* **108** 113925
[14] Hashimoto S, Ochiai Y and Aso K 1989 Perpendicular magnetic anisotropy in sputtered CoPd alloy films *Jpn. J. Appl. Phys.* **28** 1596

[15] Das S S, Kopnov G and Gerber A 2018 Detection of hydrogen by the extraordinary Hall effect in CoPd alloys *J. Appl. Phys.* **124** 104502
[16] Jen S U, Chao B L and Liu C C 1994 Hall effect of polycrystalline Co-Pd alloys *J. Appl. Phys.* **76** 5782–5
[17] Tao X *et al* 2018 Self-consistent determination of spin Hall angle and spin diffusion length in Pt and Pd: The role of the interface spin loss *Sci. Adv.* **4** eaat1670
[18] Toyama R, Masuda K, Simalaotao K, Zhou W, Kushwaha V K and Sakuraba Y 2024 Large anomalous Nernst conductivity of L10-ordered CoPt in CoPt composition-spread thin films *J. Appl. Phys.* **57** 405001
[19] Tao X D, Feng Z, Miao B F, Sun L, You B, Wu D, Du J, Zhang W and Ding H F 2014 The spin Hall angle and spin diffusion length of Pd measured by spin pumping and microwave photoresistance *J. Appl. Phys.* **115** 17C504
[20] Tang Z, Kitamura Y, Shikoh E, Ando Y, Shinjo T and Shiraishi M 2013 Temperature dependence of spin Hall angle of palladium *Appl. Phys. Express* **6** 083001
[21] Keller S, Mihalceanu L, Schweizer M R, Lang P, Heinz B, Geilen M, Brächer T, Pirro P, Meyer T and Conca A 2018 Determination of the spin Hall angle in single-crystalline Pt films from spin pumping experiments *New J. Phys.* **20** 053002
[22] Ando K, Takahashi S, Harii K, Sasage K, Ieda J, Maekawa S and Saitoh E 2008 Electric manipulation of spin relaxation using the spin Hall effect *Phys. Rev. Lett.* **101** 036601
[23] Hasegawa K, Mizuguchi M, Sakuraba Y, Kamada T, Kojima T, Kubota T, Mizukami S, Miyazaki T and Takanashi K 2015 Material dependence of anomalous Nernst effect in perpendicularly magnetized ordered-alloy thin films *Appl. Phys. Lett.* **106** 252405
[24] Takata F M and Sumodjo P T A 2007 Electrodeposition of magnetic CoPd thin films: Influence of plating condition Electrochim. Acta **52** 6089–96
[25] Uchida K, Ota T, Harii K, Takahashi S, Maekawa S, Fujikawa Y and Saitoh E 2010 Spin-Seebeck Effects in Ni81fe19/Pt Films *Solid State Commun.* **150** 524-528
[26] Sola A, Bougiatioti P, Kuepferling M, Meier D, Reiss G, Pasquale M, Kuschel T and Basso V 2017 Longitudinal spin Seebeck coefficient: heat flux vs. temperature difference method *Sci. Rep.* **7** 46752
[27] Noce R D, Barelli N, Sumodjo P T A, Cornejo D R and Benedetti A V 2006 Effect of the bath pH on the electrodeposition of nanocrystalline Pd-Co alloys and their magnetic properties *J. Magn. Magn. Mater.* **306** 199–203
[28] Chuang T C, Su P L, Wu P H and Huang S Y 2017 Enhancement of the anomalous Nernst effect in ferromagnetic thin films *Phys. Rev. B* **96** 174406
[29] Tsui L-kun, Zafferoni C, Lavacchi A, Innocenti M, Vizza F and Zangari G 2015 Electrocatalytic activity and operational stability of electrodeposited Pd-Co films towards ethanol oxidation in alkaline electrolytes *J. Power Sources* **293** 815–22